Christopher G. Atkeson
Chae H. An
John M. Hollerbach
Artificial Intelligence Laboratory
Massachusetts Institute of Technology
Cambridge, Massachusetts 02139

Estimation of Inertial Parameters of Manipulator Loads and Links

Abstract

The inertial parameters of manipulator rigid-body loads and links have been automatically estimated as a result of general movement. The Newton-Euler equations have been recast to relate linearly the measured joint forces or torques via acceleration-dependent coefficients to the inertial parameters, which have then been estimated by least squares. Load estimation was implemented on a PUMA 600 robot equipped with an RTI FS-B wrist force-torque sensor and on the MIT Serial Link Direct Drive Arm equipped with a Barry Wright Company Astek wrist force-torque sensor. Good estimates were obtained for load mass and center of mass, and the forces and torques due to movement of the load could be predicted accurately. The load moments of inertia were more difficult to estimate. Link estimation was implemented on the MIT Serial Link Direct Drive Arm. A good match was obtained between joint torques predicted from the estimated parameters and the joint torques estimated from motor currents. The match actually proved superior to predicted torques based on link inertial parameters derived by CAD modeling. Restrictions on the identifiability of link inertial parameters due to restricted sensing and movement near the base have been addressed. Implications of estimation accuracy for manipulator dynamics and control have been considered.

This paper describes research done at the Artificial Intelligence Laboratory of the Massachusetts Institute of Technology. Support for the laboratory's artificial intelligence research is provided in part by the Systems Development Foundation and the Defense Advanced Research Projects Agency under Office of Naval Research contracts N00014-80-C-050 and N00014-82-K-0334. Partial support for C. Atkeson was provided by a Whitaker Fund Graduate Fellowship, for C. An by an NSF Graduate Fellowship, and for J. Hollerbach by an NSF Presidential Young Investigator Award.

The International Journal of Robotics Research,
Vol. 5, No. 3, Fall 1986,

1. Introduction

Knowledge of the inertial parameters of manipulator loads and links (mass, center of mass, and moments of inertia) is potentially important for precise control of movement. For the link inertial parameters, not even the robot manufacturers typically know their values. Robot manipulators are designed according to precise kinematic specifications, but the link inertial parameters are incidental attributes of design. Because the robust controllers usually provided by the manufacturers do not take link dynamics into account, there is no inducement to determine these parameters. Even if a determination were attempted, the usual method of disassembling the robot and painstakingly weighing and balancing the components is complex and time-consuming. Another method involves entering a computer model of the arm into a CAD/CAM database, but the accuracy of these models is not clear.

Load inertial parameters must be redetermined every time a new load is picked up. In terms of trajectory control, it may be necessary to incorporate the load inertial parameters into the inertial parameters of the last link. In addition, the load inertial parameters are an integral part of the grasped object's description, just as surely as are the geometrical parameters. Hence load identification can assist object recognition. Moreover, the estimated location of the center of mass and the orientation of the principal axes of inertia can be used to verify that the manipulator has grasped the object in the desired manner.

In this paper we present a procedure that estimates load and link inertial parameters as a result of general movement; the loads and links are considered to be rigid bodies. Forces or torques measured at the joints are related to kinematic measurements of position, velocity, and acceleration. Although the dynamic equations are nonlinear, the inertial parameters of

mass, center of mass, and moments of inertia appear linearly in the Newton-Euler equations. Hence a standard least-squares estimation procedure may be used to average many data points and compensate for noise.

Unlike previous efforts that presented only equations or sometimes simulations, our approach has been verified experimentally on robot arms. Thus we are able to determine how well these parameters can be estimated, given sources of noise in sensors and in signal processing and limitations in robot acceleratory ability. Also, we have characterized which link inertial parameters can be separately identified or must be identified in linear combinations, given limitations on sensing and restrictions on movement near the manipulator base.

Load estimation was implemented on a PUMA 600 robot equipped with an RTI FS-B wrist force-torque sensor and on the MIT Serial Link Direct Drive Arm equipped with a Barry Wright Company Astek wrist force-torque sensor. These force-torque sensors measure all six components of force and torque resulting from gravity loading and acceleration of hand plus load. Although torque sensing at the joints could in principle yield the same information, the wrist sensor measurements are more accurate.

Link estimation was implemented on the MIT Serial Link Direct Drive Arm. Unlike load estimation, the only sensing is one component of joint torque, inferred from motor current. Coupled with restricted movement near the base, it is not possible to find all the inertial parameters of the proximal links. As will be seen, these missing parameters have no effect on the control of the arm.

1.1. Relation to Previous Work

1.1.1. Load Estimation

Paul (1981) described two methods of determining the mass of a load when the manipulator is at rest. One method requires the knowledge of joint torques and the other method requires knowledge of forces and torques at the wrist. The center of mass and the load moments of inertia were not identified.

Coiffet (1983) utilized joint torque sensing to estimate the mass and center of mass of a load for a robot at rest. Moments of inertia were estimated with special test motions, moving only one axis at a time or applying test torques. Because of the intervening link masses and domination of inertia by the mass moments, joint torque sensing is less accurate than wrist force-torque sensing.

Olsen and Bekey (1985) assumed full force-torque sensing at the wrist to identify the load without special test motions. Mukerjee (1984) and Mukerjee and Ballard (1985) developed an approach similar to ours, again allowing general motion during load identification. Nevertheless, neither paper simulated or experimentally implemented their procedures to verify the correctness of the equations or to determine the accuracy of estimation in the presence of noise and imperfect measurements.

1.1.2. Link Estimation

Mayeda, Osuka, and Kangawa (1984) required three sets of special test motions to estimate the coefficients of a closed-form Lagrangian dynamics formulation. The ten inertial parameters of each link are lumped into these numerous coefficients, which are redundant and susceptible to numerical problems in estimation. On the other hand, every coefficient is identifiable since these coefficients represent the actual degrees of freedom of the robot. By sensing torque from only one joint at a time, their algorithm is more susceptible to noise from transmission of dynamic effects of distant links to the proximal measuring joints. For efficient dynamics computation, the recursive dynamics algorithms require the link parameters explicitly. Though recoverable from the Lagrangian coefficients, it is better to estimate the inertial parameters directly. Though this algorithm was implemented on a PUMA robot, it is hard to interpret the results because of dominance of the dynamics by the rotor inertia and friction.

Mukerjee (1984) and Mukerjee and Ballard (1985) directly applied their load identification method to link identification by requiring full force-torque sensing at each joint. Instrumenting each robot link with full force-torque sensing seems impractical, and is actually unnecessary given joint-torque sensing about the rotation axis. Partially as a result, they do not address the issue of unidentifiability of some inertial

parameters. As with load identification, the algorithm was not verified by simulation or by implementation.

Olsen and Bekey (1985) presented a link identification procedure using joint-torque sensing and special test motions with single joints. The unidentifiability of certain inertial parameters was not resolved, and the least-squares estimation procedure written as a generalized inverse would fail because of linear dependence of some of the inertial parameters. Again, their procedure was not tested by simulation or by actual implementation on a robot arm.

Neuman and Khosia (1985) developed a hybrid estimation procedure combining a Newton-Euler and a Lagrange-Euler formulation of dynamics. Simulation results for a three-degree-of-freedom cylindrical robot were presented, and the unidentifiability of certain inertial components was addressed. For some reason, knowledge of link mass for a linear estimation procedure was required, but such a restriction does not exist with our method. Although planning to work with the Carnegie-Mellon University Direct Drive Arm II, Neuman and Khosia were not yet able to present experimental results.

2. A Newton-Euler Estimation Procedure

The same underlying formulation based on the Newton-Euler equations serves for both rigid-body load and link estimation. Each link of a manipulator is considered in isolation, and the force of inertia exerted on the proximal joint is derived from the acceleration of the link. This formulation will first be applied to *load estimation,* which is tantamount to estimation for the last link of the manipulator alone. Load estimation is also conceptually simpler than link estimation because of the presence of full force-torque sensing at the wrist and general movement of the load. *Link estimation* will be treated next, in which only one component of force or torque is sensed and in which proximal links do not experience general movement. The force of inertia from distal links must be summed and transmitted to the proximal links.

In this paper, we only discuss manipulators with revolute joints since handling prismatic joints requires only trivial modifications to the algorithms. Beginning with an n-joint manipulator, we assume each link i

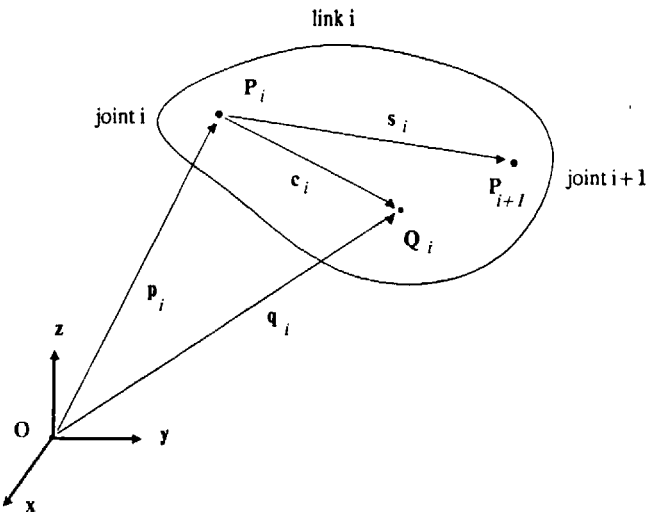

Fig. 1. Coordinate origins and location vectors for link and load identification.

has a local coordinate system $\mathbf{P}_i$ with the origin fixed at joint i; the vector $\mathbf{p}_i$ locates $\mathbf{P}_i$ with respect to a global coordinate system $\mathbf{O}$ (Fig. 1). At the center of mass, a coordinate system $\mathbf{Q}_i$ is aligned with the principal axes of inertia. The center of mass is located with respect to $\mathbf{P}_i$ by the vector $\mathbf{c}_i$ and with respect to the global origin $\mathbf{O}$ by $\mathbf{q}_i$.

The inertial parameters of mass, center of mass, and moment of inertia are related to the motion of link i by the Newton-Euler equations:

$$ {}_q\mathbf{f}_i = \mathbf{f}_{ii} + m_i\mathbf{g} = m_i\ddot{\mathbf{q}}_i, \tag{1} $$

$$ {}_q\mathbf{n}_i = \mathbf{n}_{ii} - \mathbf{c}_i \times \mathbf{f}_{ii} = {}_q\mathbf{I}_i\dot{\boldsymbol{\omega}}_i + \boldsymbol{\omega}_i \times ({}_q\mathbf{I}_i\boldsymbol{\omega}_i), \tag{2} $$

where

${}_q\mathbf{f}_i$ = the net force acting on link i,
${}_q\mathbf{n}_i$ = the net torque about the center of mass of link i,
$\mathbf{f}_{ij}$ = the force at joint i due to motion of link j alone,
$\mathbf{n}_{ij}$ = the torque at joint i due to motion of link j alone,
m_i = the mass of link i,
${}_q\mathbf{I}_i$ = the moment of inertia about the center of mass,
$\boldsymbol{\omega}_i$ = the angular velocity vector, and
$\mathbf{g}$ = the gravity vector $\mathbf{g} = [0, 0, -9.8\ \text{m/sec}^2]$.

Although the location of the center of mass and hence its acceleration $\ddot{\mathbf{q}}_i$ are unknown, Symon (1971)

related the latter to the acceleration $\ddot{\mathbf{p}}_i$ of joint i by

$$\ddot{\mathbf{q}}_i = \ddot{\mathbf{p}}_i + \dot{\boldsymbol{\omega}}_i \times \mathbf{c}_i + \boldsymbol{\omega}_i \times (\boldsymbol{\omega}_i \times \mathbf{c}_i). \tag{3}$$

Substituting into Eq. (1), which then substitutes into Eq. (2), we get

$$\mathbf{f}_{ii} = m_i(\ddot{\mathbf{p}}_i - \mathbf{g}) + \dot{\boldsymbol{\omega}}_i \times m_i\mathbf{c}_i + \boldsymbol{\omega}_i \times (\boldsymbol{\omega}_i \times m_i\mathbf{c}_i), \tag{4}$$

$$\begin{aligned}\mathbf{n}_{ii} = {} & (\mathbf{g} - \ddot{\mathbf{p}}_i) \times m_i\mathbf{c}_i + {}_q\mathbf{I}_i\dot{\boldsymbol{\omega}}_i + m\mathbf{c}_i \times (\dot{\boldsymbol{\omega}}_i \times \mathbf{c}_i) \\ & + \boldsymbol{\omega}_i \times ({}_q\mathbf{I}_i\boldsymbol{\omega}_i) + m_i\mathbf{c}_i \times (\boldsymbol{\omega}_i \times (\boldsymbol{\omega}_i \times \mathbf{c}_i)).\end{aligned} \tag{5}$$

Although the terms $\mathbf{c}_i \times (\dot{\boldsymbol{\omega}}_i \times \mathbf{c}_i)$ and $\mathbf{c}_i \times (\boldsymbol{\omega}_i \times (\boldsymbol{\omega}_i \times \mathbf{c}_i))$ are quadratic in the unknown location of the center of mass $\mathbf{c}_i$, they may be eliminated by expressing the moment-of-inertia tensor about the joint i origin ${}_p\mathbf{I}_i$ instead of about the center of mass ${}_q\mathbf{I}_i$. By the parallel axis theorem, Symon (1971) shows that

$${}_p\mathbf{I}_i = {}_q\mathbf{I}_i + m_i[(\mathbf{c}_i^T\mathbf{c}_i)\mathbf{1} - (\mathbf{c}_i\mathbf{c}_i^T)] \tag{6}$$

where $\mathbf{1}$ is the 3-D identity matrix. Rewriting Eq. (5) and substituting, we get

$$\begin{aligned}\mathbf{n}_{ii} = {} & (\mathbf{g} - \ddot{\mathbf{p}}_i) \times m_i\mathbf{c}_i + {}_q\mathbf{I}_i\dot{\boldsymbol{\omega}}_i \\ & + m_i[(\mathbf{c}_i^T\mathbf{c}_i)\mathbf{1} - (\mathbf{c}_i\mathbf{c}_i^T)]\dot{\boldsymbol{\omega}}_i \\ & + \boldsymbol{\omega}_i \times ({}_q\mathbf{I}_i\boldsymbol{\omega}_i) + \boldsymbol{\omega}_i \times (m_i[(\mathbf{c}_i^T\mathbf{c}_i)\mathbf{1} - (\mathbf{c}_i\mathbf{c}_i^T)]\boldsymbol{\omega}_i) \\ = {} & (\mathbf{g} - \ddot{\mathbf{p}}_i) \times m_i\mathbf{c}_i + {}_p\mathbf{I}_i\dot{\boldsymbol{\omega}}_i + \boldsymbol{\omega}_i \times ({}_p\mathbf{I}_i\boldsymbol{\omega}_i).\end{aligned} \tag{7}$$

The following notation is used to formulate a system of linear equations from the preceding ones:

$$\boldsymbol{\omega} \times \mathbf{c} = \begin{bmatrix} 0 & -\omega_z & \omega_y \\ \omega_z & 0 & -\omega_x \\ -\omega_y & \omega_x & 0 \end{bmatrix} \begin{bmatrix} c_x \\ c_y \\ c_z \end{bmatrix} \triangleq [\boldsymbol{\omega}\times]\,\mathbf{c},$$

$$\mathbf{I}\boldsymbol{\omega} = \begin{bmatrix} \omega_x & \omega_y & \omega_z & 0 & 0 & 0 \\ 0 & \omega_x & 0 & \omega_y & \omega_z & 0 \\ 0 & 0 & \omega_x & 0 & \omega_y & \omega_z \end{bmatrix} \begin{bmatrix} I_{xx} \\ I_{xy} \\ I_{xz} \\ I_{yy} \\ I_{yz} \\ I_{zz} \end{bmatrix}$$

$$\triangleq [\cdot\,\boldsymbol{\omega}] \begin{bmatrix} I_{xx} \\ I_{xy} \\ I_{xz} \\ I_{yy} \\ I_{yz} \\ I_{zz} \end{bmatrix},$$

where

$$\mathbf{I} = \mathbf{I}^T = \begin{bmatrix} I_{xx} & I_{xy} & I_{xz} \\ I_{xy} & I_{yy} & I_{yz} \\ I_{xz} & I_{yz} & I_{zz} \end{bmatrix}.$$

A matrix equation can now be written from Eqs. (4) and (7) as

$$\begin{bmatrix} \mathbf{f}_{ii} \\ \mathbf{n}_{ii} \end{bmatrix} = \begin{bmatrix} \ddot{\mathbf{p}}_i - \mathbf{g} & [\dot{\boldsymbol{\omega}}_i\times] + [\boldsymbol{\omega}_i\times][\boldsymbol{\omega}_i\times] & \mathbf{0} \\ \mathbf{0} & [(\mathbf{g} - \ddot{\mathbf{p}}_i)\times] & [\cdot\,\dot{\boldsymbol{\omega}}_i] + [\boldsymbol{\omega}_i\times][\cdot\,\boldsymbol{\omega}_i] \end{bmatrix} \times \begin{bmatrix} m_i \\ m_i\mathbf{c}_i \\ I_{xx_i} \\ I_{xy_i} \\ I_{xz_i} \\ I_{yy_i} \\ I_{yz_i} \\ I_{zz_i} \end{bmatrix}$$

or more compactly as

$$\boldsymbol{w}_{ii} = \boldsymbol{A}_i\boldsymbol{\phi}_i, \tag{8}$$

where $\boldsymbol{w}_{ij}$ is the six-element wrench at joint i due to the movement of link j alone, $\boldsymbol{A}_i$ is a 6×10 matrix, and $\boldsymbol{\phi}_i$ is the vector of the ten unknown inertial parameters. Note that the center of mass cannot be determined directly but only as the mass moment $m_i\mathbf{c}_i$. But since the mass m_i is separately determined, its contribution can be factored from the mass moment later, if necessary.

2.1. Load Estimation

When a rigid load is picked up, it becomes an integral part of the last link or hand. Hence load estimation is equivalent to estimation of the altered inertial parameters of the last link n. With a wrist force-torque sensor, all elements of the wrench $\boldsymbol{w}_{nn}$ can be directly mea-

sured. The quantities inside the A_n matrix are computed from the direct kinematics and the measured joint angles (Luh, Walker, and Paul 1980*a*).

Since Eq. (8) represents six equations and ten unknowns, the wrench must be sampled in at least two different manipulator configurations to solve for ϕ_n, but more configurations would be desirable because of noise. Each data point adds six more equations, and N data points can be represented by augmenting w_{nn} and A_n as shown below:

$$\mathbf{A} = \begin{bmatrix} A_n(1) \\ \cdot \\ \cdot \\ \cdot \\ A_n(N) \end{bmatrix}, \qquad \mathbf{w} = \begin{bmatrix} w_{nn}(1) \\ \cdot \\ \cdot \\ \cdot \\ w_{nn}(N) \end{bmatrix}.$$

A simple least-squares estimation yields

$$\hat{\phi}_n = (\mathbf{A}^T\mathbf{A})^{-1}\mathbf{A}^T\mathbf{w}. \tag{9}$$

For an on-line estimation, Eq. (9) can also be formulated in a recursive form (Ljung and Soderstrom 1983).

2.1.1. Recovering Object And Grip Parameters

The estimated inertial parameters (m_n, $m_n\mathbf{c}_n$, ${}_p\mathbf{I}_n$) are adequate for control, but grasp verification and object recognition require the location of the center of mass $\mathbf{c}_n$, the principal moments of inertia I_1, I_2, I_3 about the center of mass, and the orientation ${}_{qp}\hat{\mathbf{R}}_n$ of $\mathbf{Q}_n$ with respect to $\mathbf{P}_n$.

The parallel axis theorem is used to compute the inertia terms translated to the center of mass of the load as follows:

$$\begin{aligned} \hat{\mathbf{c}}_n &= \frac{m_n\mathbf{c}_n}{\hat{m}_n}, \\ {}_q\hat{\mathbf{I}}_n &= {}_p\hat{\mathbf{I}}_n - \hat{m}_n[(\hat{\mathbf{c}}_n^T\hat{\mathbf{c}}_n)\mathbf{1} - (\hat{\mathbf{c}}_n\hat{\mathbf{c}}_n^T)]. \end{aligned} \tag{10}$$

The principal moments are obtained by diagonalizing ${}_q\hat{\mathbf{I}}_n$ as follows:

$${}_q\hat{\mathbf{I}}_n = {}_{qp}\hat{\mathbf{R}}_n \begin{bmatrix} \hat{I}_1 & 0 & 0 \\ 0 & \hat{I}_2 & 0 \\ 0 & 0 & \hat{I}_3 \end{bmatrix} {}_{qp}\hat{\mathbf{R}}_n^T. \tag{11}$$

This diagonalization can always be achieved since ${}_q\hat{\mathbf{I}}_n$ is symmetric, but when two or more principal moments are equal, the rotation matrix ${}_{qp}\hat{\mathbf{R}}_n$ is no longer unique.

2.2. Link Estimation

For link estimation, the total wrench $\mathbf{w}_i$ at joint i must be determined by summing the wrenches w_{ij} for all links j distal to joint i:

$$\mathbf{w}_i = \sum_{j=i}^{N} w_{ij}. \tag{12}$$

First, each distal wrench w_{jj} must be transmitted across intermediate joints to reflect its contribution w_{ij} at joint i. This is a function of the geometry of the linkage only. The forces and torques at neighboring joints are related by

$$\begin{bmatrix} \mathbf{f}_{i,i+1} \\ \mathbf{n}_{i,i+1} \end{bmatrix} = \begin{bmatrix} \mathbf{R}_i & \mathbf{0} \\ [\mathbf{s}_i\times]\cdot\mathbf{R}_i & \mathbf{R}_i \end{bmatrix} \begin{bmatrix} \mathbf{f}_{i+1,i+1} \\ \mathbf{n}_{i+1,i+1} \end{bmatrix}, \tag{13}$$

or more compactly

$$w_{i,i+1} = \mathbf{T}_i w_{i+1,i+1}, \tag{14}$$

where

$\mathbf{R}_i$ = the rotation matrix rotating the link $i+1$ coordinate system to the link i coordinate system,
$\mathbf{s}_i$ = a vector from the origin of the link i coordinate system to the link $i+1$ coordinate system, and
$\mathbf{T}_i$ = a wrench transmission matrix.

To obtain the forces and torques at the i^{th} joint due to the movements of the j^{th} link, these matrices can be cascaded as follows:

$$w_{ij} = \mathbf{T}_i\mathbf{T}_{i+1}\cdots\mathbf{T}_j w_{jj} = \mathbf{U}_{ij}\phi_j, \tag{15}$$

where $\mathbf{U}_{ij} = \mathbf{T}_i\mathbf{T}_{i+1}\cdots\mathbf{T}_j A_i$ and $\mathbf{U}_{ii} = A_i$. A simple matrix expression for a serial kinematic chain (in this case a six-joint arm) can be derived from Eqs. (12)

and (15):

$$\begin{bmatrix} \mathbf{w}_1 \\ \mathbf{w}_2 \\ \mathbf{w}_3 \\ \mathbf{w}_4 \\ \mathbf{w}_5 \\ \mathbf{w}_6 \end{bmatrix} = \begin{bmatrix} \mathbf{U}_{11} & \mathbf{U}_{12} & \mathbf{U}_{13} & \mathbf{U}_{14} & \mathbf{U}_{15} & \mathbf{U}_{16} \\ \mathbf{0} & \mathbf{U}_{22} & \mathbf{U}_{23} & \mathbf{U}_{24} & \mathbf{U}_{25} & \mathbf{U}_{26} \\ \mathbf{0} & \mathbf{0} & \mathbf{U}_{33} & \mathbf{U}_{34} & \mathbf{U}_{35} & \mathbf{U}_{36} \\ \mathbf{0} & \mathbf{0} & \mathbf{0} & \mathbf{U}_{44} & \mathbf{U}_{45} & \mathbf{U}_{46} \\ \mathbf{0} & \mathbf{0} & \mathbf{0} & \mathbf{0} & \mathbf{U}_{55} & \mathbf{U}_{56} \\ \mathbf{0} & \mathbf{0} & \mathbf{0} & \mathbf{0} & \mathbf{0} & \mathbf{U}_{66} \end{bmatrix} \begin{bmatrix} \phi_1 \\ \phi_2 \\ \phi_3 \\ \phi_4 \\ \phi_5 \\ \phi_6 \end{bmatrix}. \quad (16)$$

This equation is linear in the unknown parameters, but the left side is composed of a full force-torque vector at each joint. Since only the torque about the joint axis can usually be measured, each joint wrench must be projected onto the joint rotation axis (typically [0, 0, 1] in internal coordinates), reducing Eq. (16) to

$$\tau = \boldsymbol{K}\psi \quad (17)$$

where $\tau_i = [0, 0, 0, 0, 0, 1] \cdot \mathbf{w}_i$ is the joint torque of the i^{th} link, $\psi_i = \phi_i$, and $\boldsymbol{K}_{ij} = [0, 0, 0, 0, 0, 1] \cdot \mathbf{U}_{ij}$ when the corresponding entry in Eq. (16) is nonzero.

2.2.1. *Estimating the Link Parameters*

As with load identification, Eq. (17) is augmented using N data points:

$$\mathbf{K} = \begin{bmatrix} \boldsymbol{K}(1) \\ \cdot \\ \cdot \\ \cdot \\ \boldsymbol{K}(N) \end{bmatrix}, \qquad \tau = \begin{bmatrix} \tau(1) \\ \cdot \\ \cdot \\ \cdot \\ \tau(N) \end{bmatrix}. \quad (18)$$

Unfortunately, one cannot proceed as before with a least-squares estimate:

$$\psi_{estimate} = (\mathbf{K}^T\mathbf{K})^{-1}\mathbf{K}^T\tau \quad (19)$$

because $\mathbf{K}^T\mathbf{K}$ is not invertible due to loss of rank from restricted degrees of freedom at the proximal links and the lack of full force-torque sensing. Some inertial parameters are completely unidentifiable, while others can only be identified in linear combinations.

Two different approaches were used to solve the preceding rank-deficient problem. The simplest approach was *ridge regression* (Marquardt and Snee 1975), which made $\mathbf{K}^T\mathbf{K}$ invertible by adding a small number d to the diagonal elements:

$$\hat{\psi} = (\mathbf{K}^T\mathbf{K} + d\mathbf{I}_{10n})^{-1}\mathbf{K}^T\tau. \quad (20)$$

The estimates are nearly optimal if $d \ll \lambda_{min}(\mathbf{K}^T\mathbf{K})$, where λ_{min} is the smallest nonzero eigenvalue of $\mathbf{K}^T\mathbf{K}$.

The second approach expresses the dynamics in terms of a reduced set of inertial parameters that are independently identifiable and that allow the application of a straight least-squares estimate. This reduced set can be generated either by examination of the closed-form dynamic equations for linear combinations of parameters or by application of singular-value decomposition. Both methods were applied and the results checked against each other. The closed-form equations were derived with the aid of MACSYMA (Mathlab Group 1983) for the MIT Serial Link Direct Drive Arm, since for three degrees of freedom the dynamic equations in closed form are already quite complicated. The results are summarized in Appendix I in terms of 15 essential variables. Both the unidentifiable parameters and the parameters identifiable only in linear combinations are made explicit.

Singular value decomposition of $\mathbf{K}$ in Eq. (18) is a far less complicated method that can be applied rather automatically to any manipulator kinematic structure (Golub and Van Loan 1983):

$$\mathbf{K} = \mathbf{U}\Sigma\mathbf{V}^T,$$

where $\Sigma = \text{diag}\{\sigma_i\}$ and $\mathbf{U}$ and $\mathbf{V}^T$ are orthogonal matrices. For each column of $\mathbf{V}$ there is a corresponding nonzero singular value σ_i, indicating that the linear combination of parameters, $\mathbf{v}_i^T\psi$, is identifiable. The unidentifiable parameters will have zero singular values associated with them. Since $\mathbf{K}$ is a function only of the geometry of the arm and the commanded movement, it can be generated exactly by simulation rather than by actually moving the real arm and recording data with the concomitant and inevitable noise. For completely unidentifiable parameters, the corresponding columns of $\mathbf{K}$ can be deleted without affecting τ. For parameters identifiable in linear combinations, all columns except one in a linear combination can also be deleted. The resulting smaller $\mathbf{K}^T\mathbf{K}$

Fig. 2. PUMA with a test load.

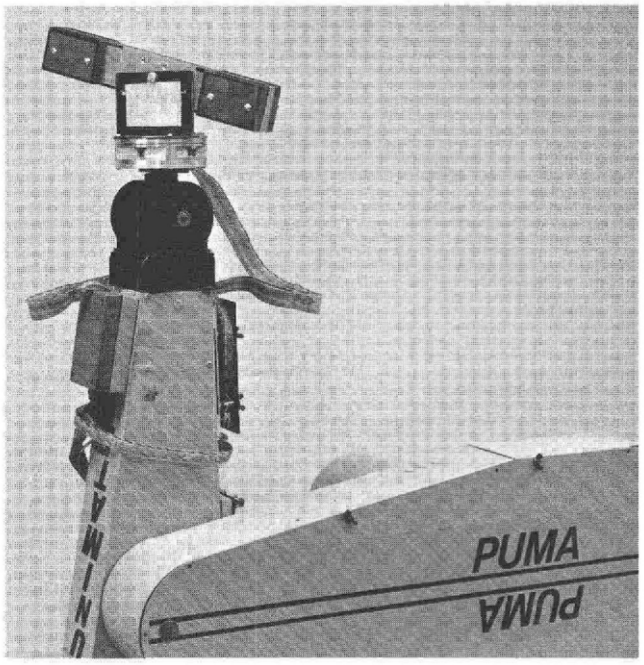

Fig. 3. Measured angle θ, calculated angular velocity $\dot{\theta}$, and calculated angular acceleration $\ddot{\theta}$ for joint 4.

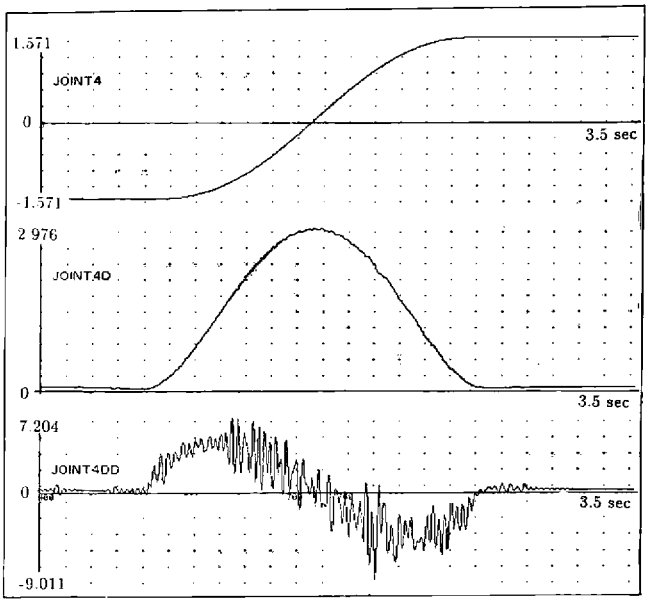

matrix will be invertible, and Eq. (19) can be used to estimate the reduced set of parameters.

3. Experimental Results

3.1. Rigid-Body Load Estimation on the PUMA Robot

Rigid-body load estimation was originally implemented on a PUMA 600 robot equipped with an RTI FS-B wrist force-torque sensor (Fig. 2). Joint velocities and accelerations were obtained through differentiation of joint-angle encoder readings (Fig. 3). A cutoff frequency of 33 Hz for the filter was determined experimentally to include all of the structural resonant frequencies of the manipulator, and a data sampling rate of 200 Hz was found sufficient.

3.1.1. Static Load Estimation Using the PUMA

The mass and center of mass were estimated first statically and then dynamically as a result of movement. A static estimation basically tests the calibration of the wrist sensor and of the kinematics of the PUMA arm. The wrist forces and torques are now due only to gravity:

$$\begin{aligned} \mathbf{f}_{nn} &= -m_n \mathbf{g}, \\ \mathbf{n}_{nn} &= -m_n \mathbf{c}_n \times \mathbf{g}. \end{aligned} \tag{21}$$

Thus only the mass and the center of mass can be identified while the manipulator is stationary.

The inertial parameter estimates of the last link include contributions from the gripper plus load. Thus the gripper contribution would have to be subtracted from the link estimates to determine the load mass and center of mass. This is simple for mass but difficult for center of mass, since the gripper is complicated and its center of mass is not known. We sought a way to verify the estimation accuracy for the load center of mass while circumventing the need for knowledge of the gripper center of mass. This was done by moving the load along the gripper approach axis (the y-axis) by known amounts and tracking the change in the center of mass.

The static estimates are shown in the second column of Table 1 for an aluminum block ($2 \times 2 \times 6$ in.) with a mass of 1.106 kg. For the center of mass, only the changes in c_y are shown; the estimates of c_x and c_z remained within 1 mm of the reference values ($c_x =$

Table 1. Mass and the Center of Mass Estimates

Parameters	Actual	Static	Dynamic
Mass (kg)	1.106	1.103	1.067
Change in $c_x(m)$	0.037	0.037	0.039
Mass (kg)	1.106	1.107	1.084
Change in $c_y(m)$	−0.043	−0.043	−0.042
Mass (kg)	1.106	1.100	1.073
Change in $c_y(m)$	−0.021	−0.020	−0.021
Mass (kg)	1.106	1.099	1.074
Change in $c_y(m)$	0.018	0.018	0.020

Table 2. Actual and Estimated Moments of Inertia, Either for all Joints Moving[1] or Special Test Motions[2]

Parameters ($kg \cdot m^2$)	Actual Values	PUMA[1] Estimates	PUMA[2] Estimates	DDA[1] Estimates
I_{xx}	0.0244	0.0192	0.0246	0.0230
I_{xy}	0	−0.0048	0.0006	0.0006
I_{xz}	0	0.0019	0.0008	0.0005
I_{yy}	0.0007	0.0021	0.0036	−0.0002
I_{yz}	0	−0.0016	−0.0004	−0.0002
I_{zz}	0.0242	0.0176	0.0199	0.0241

1 mm, $c_z = 47$ mm). Each set of estimates was computed from data taken at six different positions and orientations of the manipulator, where at a given location 1000 samples were averaged to minimize the effects of noise. As seen from column 3, the load mass has been estimated to within 10 g and the load center of mass to within 1 mm.

Static load estimation only tests the force sensor calibration and the position measurement capabilities of the robot on which the sensor is mounted. In order to assess the effects of the dynamic capabilities of the robot on load estimation and to be able to estimate the moments of inertia of the load we must assess parameter estimation during general movement.

3.1.2. Dynamic Load Estimation Using the PUMA

In the dynamic case, the encoder and the wrist sensor data are sampled while the manipulator is in motion. A fifth-order polynomial trajectory (minimum-jerk time function) in joint space was used to minimize the mechanical vibrations at the beginning and the end of the movement and to improve the signal to noise ratio (SNR) in the acceleration data (Fig. 3). For the more popular bang-coast-bang trajectories, the joint accelerations are zero except at the beginning and the end of the movements, resulting in a poor SNR in the acceleration data for most of the movement. The manipulator moved from [0, 0, 0, −90, 0, 0] to [90, −60, 90, 90, 90, 90] degrees on a straight line in joint space in 2 s. Joint 4 of the PUMA has a higher maximum acceleration than the other joints, so it was given a longer path. The PUMA can move no faster along this fifth-order trajectory without exceeding some joint's maximum acceleration. The estimates used all 400 data points sampled during the movement.

The dynamic estimates of mass and center of mass for the same load are shown in the last column of Table 1. The estimates have deteriorated slightly compared to the static estimates, but are still within 40 g of the actual mass and 2 mm of the center-of-mass displacement.

3.1.3. Estimating the Moments of Inertia Using the PUMA

Unfortunately, the SNR's in the acceleration and force-torque data were too low for accurate inertia estimates (0.00238 kg · m² for the largest principal moment). The torque due to gravity is approximately 40 times greater than the torque due to the maximum angular acceleration of the load. Thus, even slight noise in the data would result in poor estimates of ${}_q\mathbf{I}_n$.

To achieve some results for inertia estimation, a new load had to be fashioned with larger inertias. Two large masses were placed at the ends of an aluminum bar (Fig. 2), yielding large moments in two directions of ~0.024 kg · m² and a small moment in the third. Unlike the tracking procedure for estimating the center of mass, here we determined the absolute load inertias by first determining the gripper inertias and subtracting them from the last link inertias. The results in Table 2 for the same trajectory contain some errors but are fairly close to the actual values.

To improve the SNR in both the acceleration and the force-torque data, special test motions were employed involving rotation about a principal axis for 2 s each. Joints 4 and 6 were used alone to achieve higher

Fig. 4. Measured force-torque data versus that computed from the estimates.

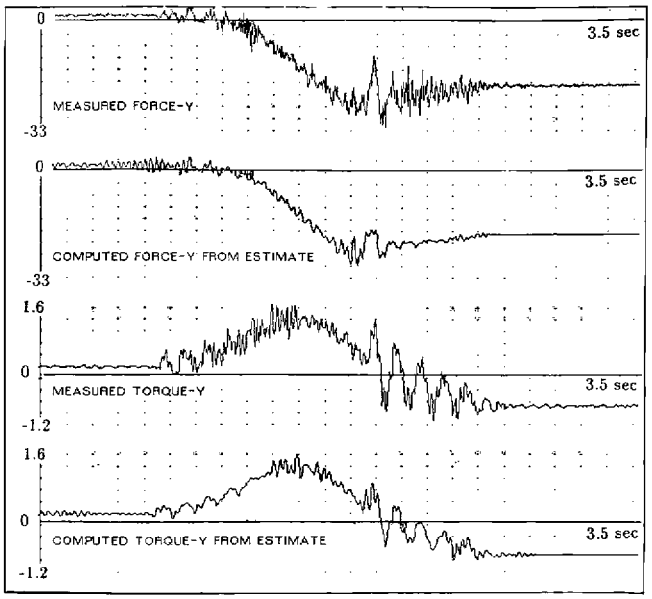

accelerations. Nearly all terms in Table 2 have improved, especially the cross terms; only I_{yy} is slightly worse. Figure 4 compares the measured forces and torques to those computed from the estimated parameters and measured joint data. The two sets of figures match very well even in the mechanical vibrations, verifying qualitatively the accuracy of the estimates. This suggests that for control purposes even poor estimation of moment-of-inertia parameters will allow good estimates of the total force and torque necessary to achieve a trajectory. This makes good sense in that the load forces with the PUMA are dominated by gravitational components, and angular accelerations experienced by the load are small relative to those components.

The effect of the errors causing poor estimates of moment-of-inertia parameters could be alleviated by increasing the angular acceleration experienced by the load. Since we had reached the sustained acceleration capacity of even an unloaded PUMA robot, we decided to explore this issue using the MIT Serial Link Direct Drive Arm. This robot can achieve higher sustained accelerations than the PUMA, and in addition it is equipped with tachometers at the joints, making estimation of acceleration much easier.

3.2. Rigid-Body Load Estimation on the MIT Serial Link Direct Drive Arm

The inertial parameter estimation algorithm was next implemented on the MIT Serial Link Direct Drive Arm (DDArm), equipped with a Barry Wright Company Astek FS6-120A-200 6-axis force-torque sensor, which again measures all three forces and three torques about a point. The DDArm is described in the link parameter estimation section that follows and is capable of higher tip velocities and accelerations than the PUMA. The DDArm has tachometers on each of its three joints so that numerical differentiation of positions is unnecessary, but we still had to digitally differentiate the velocities to find the accelerations using a cutoff frequency of 30Hz. The positions and velocities of the robot were initially sampled at a frequency of 1kHz but were later down-sampled to match the sampling frequency of the force-torque sensor of 240 Hz. The identification procedure was again implemented off-line.

The data used for estimating the inertial parameters of the load were sampled while the manipulator was moving from (280, 269.1, −30) to (80, 19.1, 220) in one second. Again a fifth-order polynomial straight line trajectory in joint space was used. The resulting estimates for the moment-of-inertia parameters are shown in the last column of Table 2. The estimates for the mass and the location of the center of mass were as good as the PUMA results and are not shown. We see that the estimated moment-of-inertia parameters are on the whole better than the PUMA results.

Parameters estimated for a set of special test movements using the DDArm were not substantially different. Our special test movements for the DDArm were not much faster than the movement of all joints, and thus probably contained the same amount of information.

Finally, Fig. 5 shows the comparison of typical measured forces and torques with computed forces and torques from the estimated parameters and the measured joint data using the simulator for the original trajectory. Once again, we have a very good match between the measured and predicted forces and torques. Thus we see that the combination of higher angular accelerations and good velocity sensing results in better parameter estimates.

Fig. 5. Measured force-torque data and computed force-torque data from the estimates using the MIT Serial Link Direct Drive Arm.

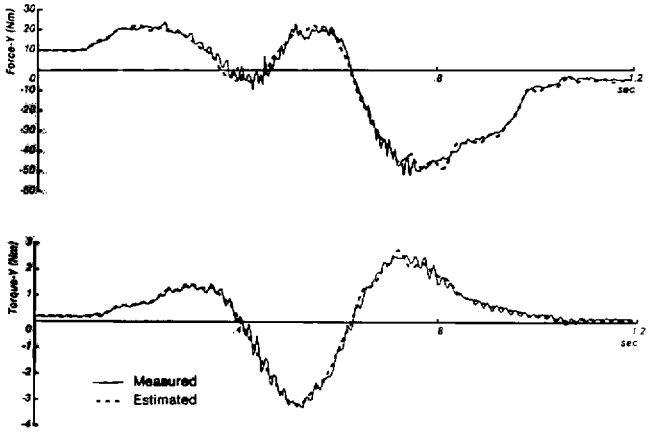

Fig. 6. MIT Serial Link Direct Drive Arm (DDArm).

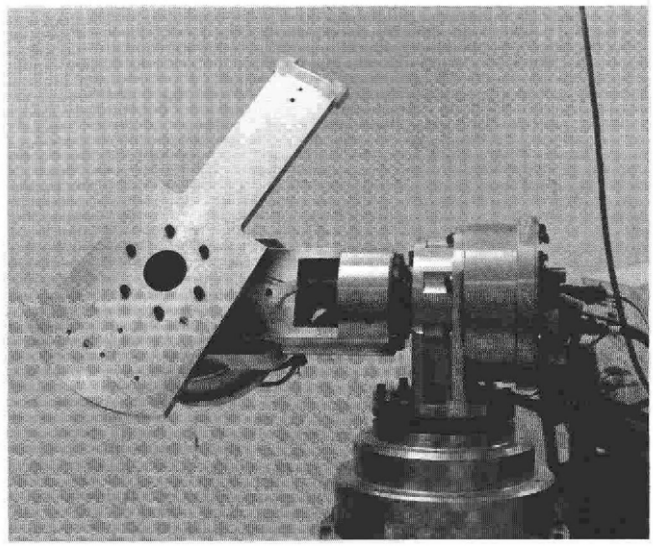

3.3. Link Estimation

Link estimation was implemented on the DDArm (Fig. 6), a three-link serial manipulator with no transmission mechanism between the motors and the links. The ideal rigid-body dynamics is a good model for this arm, uncomplicated by joint friction or backlash typical of other manipulators. Hence the fidelity of this manipulator's dynamic model well suits the estimation. The coordinate system for this arm is defined in Fig. 7. A set of inertial parameters is available for the arm (Table 3), determined by modeling with a CAD/CAM database (Lee 1983). These values can serve as a point of comparison for our method, but they may not be accurate because of modeling errors.

The motors are rated at 660 Nm peak torque for joint 1 and 230 Nm for joints 2 and 3 (Asada and Youcef-Toumi 1984). Joint 1 is presently capable of an angular acceleration of 1150 deg/s^2, joints 2 and 3 in excess of 6000 deg/s^2. In comparison, joint 1 of the PUMA 600 has a peak acceleration of 130 deg/s^2 and joint 4 at the wrist 260 deg/s^2. Joint position is measured by a resolver, and joint velocity is measured by a tachometer. The tachometer output is of high quality and leads to good acceleration estimates after differentiation. The accuracy of the acceleration estimates plus high angular accelerations greatly improve inertia estimation.

The joint torques are computed by measuring the currents of the three phase windings of each motor (Asada, Youcef-Toumi, and Lim 1984). For the three-phase, brushless, permanent magnet motors of the direct drive arm, the output torque is related to the currents in the windings by

$$\tau = K_T(I_a \sin\theta + I_b \sin(\theta + 120) + I_c \sin(\theta + 240)). \quad (22)$$

The torque constant K_T for each motor is calibrated statically by measuring the force produced by the motor torque at the end of a known lever arm. The force is measured using a Barry Wright Company Astek FS6-10A-200 six-axis force-torque sensor. Asada, Youcef-Toumi, and Lim (1984) have found

Table 3. CAD-Modeled Inertial Parameters

Parameters	Link 1	Link 2	Link 3
$m(Kg)$	67.13	53.01	19.67
$mc_x(Kg \cdot m)$	0.0	0.0	0.3108
mc_y	2.432	3.4081	0.0
mc_z	35.8257	16.6505	0.3268
$I_{xx}(Kg \cdot m^2)$	23.1568	7.9088	0.1825
I_{xy}	0.0	0.0	0.0
I_{xz}	−0.3145	0.0	−0.0166
I_{yy}	20.4472	7.6766	0.4560
I_{yz}	−1.2948	−1.5036	0.0
I_{zz}	0.7418	0.6807	0.3900

Fig. 7. The link coordinate system.

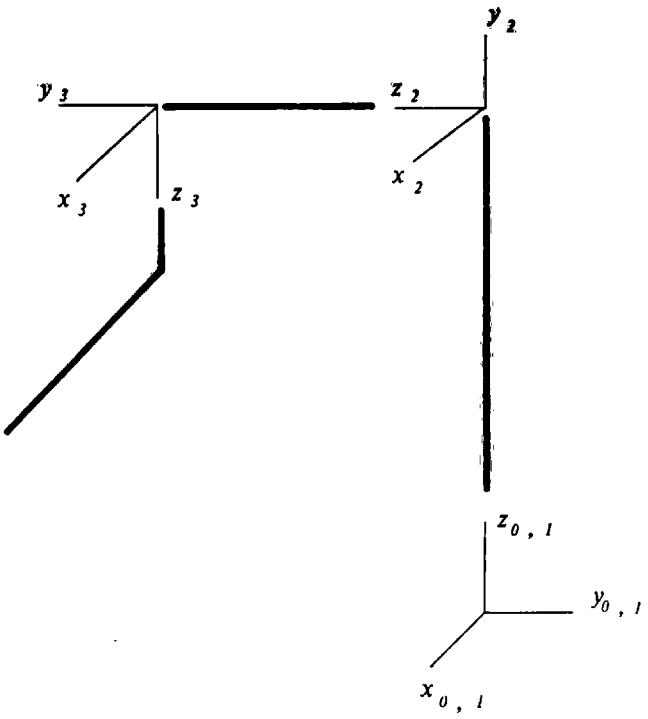

Table 4. Estimated Inertial Parameters

Parameters	Link 1	Link 2	Link 3
$m(Kg)$	0.0*	0.0*	1.8920†
$mc_x(Kg \cdot m)$	0.0*	−0.1591	0.4676
mc_y	0.0*	0.6776†	0.0315
mc_z	0.0*	0.0*	−1.0087†
$I_{xx}(Kg \cdot m^2)$	0.0*	4.1562†	1.5276†
I_{xy}	0.0*	0.3894	−0.0256
I_{xz}	0.0*	0.0118	0.0143
I_{yy}	0.0*	5.2129†	1.8967†
I_{yz}	0.0*	−0.6050†	−0.0160
I_{zz}	9.33598†	−0.8194†	0.3568

Table 5. Parameters in Linear Combinations ($l_2 = 0.45m$)

Linear Combinations	Estimated	CAD-Modeled
$m_3c_{z_3}l_2 + I_{yz_2}$	−1.0589	−1.3565
$I_{xx_3} - I_{yy_3}$	−0.3691	−0.2702
$I_{zz_2} + I_{xx_3}$	0.7082	0.8632
$I_{zz_1} + I_{xx_2} + I_{xx_3} + m_3l_2^2$	15.7029	12.8169
$I_{xx_2} + I_{xx_3} - I_{yy_2}$	0.4709	0.4147
$m_3c_{z_3} - m_2c_{y_2}$	−1.6863	−3.0814

that for a motor similar to the motors of our manipulator, the torque versus current relationship was nonlinear, especially for small magnitudes of torques, and also varied as a function of the rotor position. For the results presented in this paper, however, the nonlinear effects were ignored since substantial portions of the movements in the experiments required large magnitudes of torques. Since the least-squares algorithm minimizes the square of the error, torque errors for torques of small magnitudes do not affect the estimates very much.

For the estimation results presented, 600 data points were sampled while the manipulator was executing three sets of fifth-order polynomial trajectories in joint space. The specifications of the trajectories were:

1. (330, 289.1, 230) to (80, 39.1, −10) degrees in 1.3s,
2. (330, 269.1, −30) to (80, 19.1, 220) degrees in 1.3s,
3. (80, 269.1, −30) to (330, 19.1, 220) degrees in 1.3s.

Since $\mathbf{K}^T\mathbf{K}$ in Eq. (20) is singular, estimates can be computed either by the ridge regression method or by the reduced parameter method. Although both methods were implemented, since their results agreed with each other only the results from the ridge regression method are presented. For the ridge regression method, the estimates for the 30 unknowns are computed by adding a small number ($d = 10.0 \ll \lambda_{min}(\mathbf{K}^T\mathbf{K}) = 3395.0$) to the diagonal elements of $\mathbf{K}^T\mathbf{K}$.

Typical results are shown in Table 4. Parameters that cannot be identified because of constrained motion near the base are denoted by 0.0*. The first nine parameters of the first link are not identifiable because this link has only one degree of freedom about its z-axis. These nine parameters do not matter at all for the movement of the manipulator and thus can be arbitrarily set to 0.0.

Other parameters, marked by (†), can only be identified in linear combinations, indicated explicitly in Table 5. The ridge regression automatically resolves the linear combinations in a least-squares sense. It can

Fig. 8. The measured, the CAD-modeled, and the estimated joint torques.

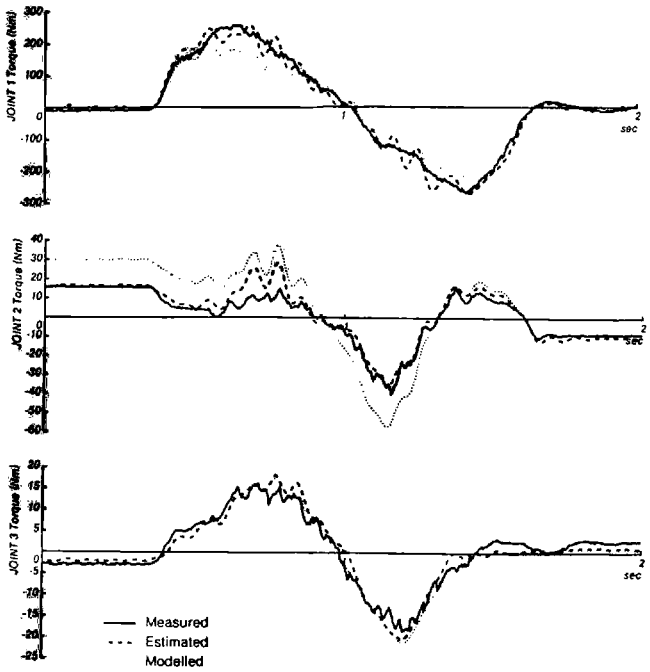

be seen that the estimated sums roughly match the corresponding sums inferred from the CAD-modeled parameters, but the sizeable discrepancy indicates that one parameter set may be more accurate than the other.

To verify the accuracy of the estimated and the modeled parameters, the measured joint torques are compared to the torques computed from the above two sets of parameters using the measured-joint kinematic data. As shown in Fig. 8, the estimated torques match the measured torques very closely. The torques computed from the CAD/CAM modeled parameters do not match the measured torques as closely. This comparison verifies qualitatively that for control purposes the estimated parameters are in fact more accurate than the CAD-modeled parameters.

4. Discussion

4.1. Load Estimation

The first part of this paper characterized the accuracy in estimating the inertial parameters of rigid body loads using wrist force/torque sensing and kinematic measurements. It was found in all cases that the mass and the location of the center of mass could be accurately estimated, either from static measurements or from measurements taken during movement. The moments of inertia were generally difficult to estimate. This distinction in estimation accuracy has different implications for control than for recognition, verification, and grasping.

For control, the gravitational torques at the wrist often dominate the dynamic torques proportional to the gripper inertia and the load inertia about the wrist. For example, a point mass executing one circular revolution in a horizontal plane, at a 5 cm radius and according to a minimum jerk-time function, must complete the motion in 425 ms for the torque due to angular acceleration to equal the gravitational torque. The gravitational torque can be accurately predicted because it depends on the mass and the location of the center of mass of the load. Even if the gripper inertia about the wrist is not accurately known, its torque contribution may be insignificant relative to gravity and hence also for control. This observation was verified by the ability to match predicted wrist forces and torques to measured values in both robot implementations (Figs. 4 and 5).

For recognition or verification, the goal is to match the estimated parameters of a grasped object to a predetermined set of parameters of known objects. In matching, the useful inertial attributes are the mass and the principal moments of inertia about the center of mass. The location of the center of mass and the orientation of the principal axes are not useful in themselves, since they are defined with respect to an arbitrary coordinate origin. Though load mass is easily determined, the principal inertias about the center of mass are not. When applying the parallel axis theorem to derive the load inertias about the center of mass from the load inertias about the wrist, the mass moment dominates the center of mass inertia. To illustrate this, the principal moment of inertia of a uniform sphere about its center is only $\frac{2}{7}$ that about an axis tangent to its surface. The effects of any errors in estimating the mass, the location of the center of mass, and the grip moments of inertia are amplified in this process. This problem would be reduced by moving the point-of-force sensing as close to the center of mass as possible. To offset partially this problem for

Fig. 9. Vibration of load on force sensor.

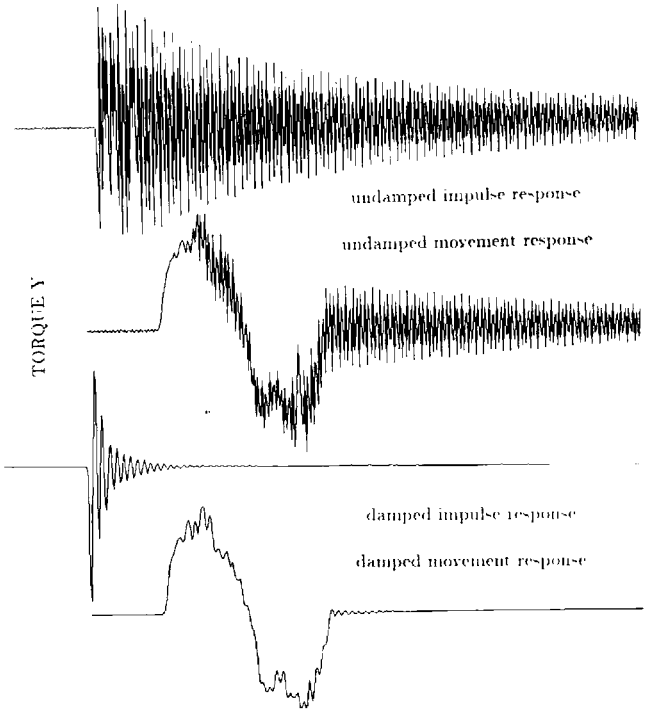

the PUMA robot, special test motions were required because of a limited acceleration capacity and the difficulty in estimating acceleration from position measurements. Such test motions were not required of the DDArm, which accelerates rapidly and has accurate joint velocity sensing.

Lastly, it is difficult to find the orientation of the principal inertia axes when they are approximately equal, even when the moments about the center of mass have been estimated accurately. Finding the orientation of the principal axes is equivalent to diagonalizing a symmetric matrix, which becomes ill-conditioned when some of the eigenvalues are almost equal. A two-dimensional example illustrates the problem. Consider the diagonalized matrix

$$\begin{bmatrix} \cos(\theta) & -\sin(\theta) \\ \sin(\theta) & \cos(\theta) \end{bmatrix} \begin{bmatrix} \lambda_1 & 0 \\ 0 & \lambda_2 \end{bmatrix} \begin{bmatrix} \cos(\theta) & \sin(\theta) \\ -\sin(\theta) & \cos(\theta) \end{bmatrix} \quad (23)$$

with eigenvalues $\{\lambda_1, \lambda_2\}$ and whose first principal axis is oriented at an angle θ with respect to the x-axis. Setting $\epsilon = \lambda_1 - \lambda_2$, Eq. (23) becomes

$$\begin{bmatrix} \lambda_2 + \epsilon \cos^2(\theta) & \epsilon \cos(\theta) \sin(\theta) \\ \epsilon \cos(\theta) \sin(\theta) & \lambda_2 + \epsilon \sin^2(\theta) \end{bmatrix}. \quad (24)$$

Thus ϵ multiplies the angle-dependent terms, which become very small when the two eigenvalues are almost equal. With a fixed amount of noise in each of the entries, the orientation θ of the principal axes becomes increasingly difficult to recover.

4.1.1. *Sources of Error*

This work is preliminary in that an adequate statistical characterization of the errors of the estimated parameters or the predicted forces has not been attempted. Possible sources of error are considered below.

Sensor Error The ultimate source of error is the random noise inherent in the sensing process itself. The noise levels in position and velocity sensing are probably negligible and could be further reduced with a model-based filter such as the Extended Kalman Filter (Gelb 1974). Force and torque is inferred from strain gauges in structural members of the sensor, and the inherent random noise is also probably negligible.

Since strain gauges are notoriously prone to drift, periodic recalibration of the offsets and of the strain-to-force calibration matrix may be necessary. Before each data collection session, our system was warmed up, and afterwards the offsets were recalibrated and rechecked.

Kinematic Errors Part of the error may be due to inaccuracies in the current kinematic parameters of the manipulator. Experiments have shown that the actual orientation of the robot can be up to 4 degrees off from the orientation computed from the encoder data.

Unmodelled Dynamics One source of unmodelled structural dynamics is flexibility in the robot links and load. Another source of greater concern is the compliance of the force sensor itself. In order to generate structural strains large enough to be measured reliably with strain gauges, a good deal of compliance is introduced into the force sensor. The load rigidly attached to the force sensor becomes a relatively undamped spring/mass system. The response of the Astek force sensor to a tap on an attached load is shown in the "undamped impulse response" record of Fig. 9. The

effect of robot movement on this spring/mass system is shown in the "undamped movement response" record.

One way to deal with wrist-sensor flexibility is to attempt to identify its dynamics. This greatly increases the complexity of the identification process and the amount of data needed for reliable estimation. We feel such an approach should only be taken as a last resort.

Another approach is to avoid exciting the unmodelled dynamics by choosing robot trajectories that are as smooth as possible. One reason for choosing fifth-order polynomial trajectories was to maintain continuity of velocities and accelerations; higher order polynomials would have resulted in even greater smoothness. Unfortunately, the PUMA still produced substantial vibration due to its hardware and the actual control methods. In fact, vibration is one way to tell if the PUMA is turned on. Vibrations were less of a problem with the DDArm, although they were still present.

The most successful approach is to damp out the vibrations mechanically by introducing some form of energy dissipation into the structure. By adding hard rubber washers between the force sensor and the load, the oscillations induced by a tap decay rapidly (Fig. 9). Similarly, the effect of movement on the resonant modes of the force sensor plus load would be reduced. We conclude that appropriate damping should be built into force sensors, just as accelerometers are filled with oil to provide a critically damped response for a specified measurement bandwidth. Failing that, energy dissipation must be introduced either into the structural components of the robot or into the gripper either structurally or as a viscous skin. Appropriate mechanical damping may also be useful in closed-loop force control.

4.1.2. Optimal Filtering

As discussed above, the numerical differentiation of velocity for acceleration greatly amplifies high frequency noise. Even worse is doubly differentiating position for acceleration. An explicit calculation of acceleration can be avoided by symbolically integrating Eqs. (4) and (7); the results, which are derived in Appendix II, are summarized below.

$$\begin{bmatrix} \int_t^{t+T} \mathbf{f}\, d\tau \\ \int_t^{t+T} \mathbf{n}\, d\tau \end{bmatrix} = \left[\int_t^{t+T} \boldsymbol{A}\, d\tau \right] \begin{bmatrix} m \\ mc_x \\ mc_y \\ mc_z \\ I_{11} \\ I_{12} \\ I_{13} \\ I_{22} \\ I_{23} \\ I_{33} \end{bmatrix}, \quad (25)$$

where the first row of $[\int_t^{t+T} \boldsymbol{A}\, d\tau]$ is

$$\left[\dot{\mathbf{p}} \Big|_t^{t+T} + \int_t^{t+T} \boldsymbol{\omega} \times \dot{\mathbf{p}}\, d\tau - \left(\int_t^{t+T} \mathbf{R}\, d\tau \right) {}^o\mathbf{g} \quad \left[\left(\boldsymbol{\omega} \Big|_t^{t+T} \right) \times \right] + \int_t^{t+T} [\boldsymbol{\omega}\times][\boldsymbol{\omega}\times] d\tau \quad \mathbf{0} \right] \quad (26)$$

and the second row is

$$\left[\mathbf{0} \left[\left(-\dot{\mathbf{p}} \Big|_t^{t+T} - \int_t^{t+T} \boldsymbol{\omega} \times \dot{\mathbf{p}}\, d\tau + \left(\int_t^{t+T} \mathbf{R}\, d\tau \right) {}^o\mathbf{g} \right) \times \right] \left[\cdot \left(\boldsymbol{\omega} \Big|_t^{t+T} \right) \right] + \int_t^{t+T} [\boldsymbol{\omega}\times][\cdot\, \boldsymbol{\omega}] d\tau \right]. \quad (27)$$

This integration approach is not necessarily the better method because it amplifies low frequency noise, such as bias in the kinematic and force data. When implemented, the integration method gave worse results in load identification with the PUMA than did the differentiation method. We are currently pursuing a method that characterizes the noise sources and filters the data optimally. This method will combine both differentiation and integration of the data so that the noises are suppressed at all frequencies.

4.2. Link Estimation

Good estimates of the link inertial parameters, based on the match of predicted torques to measured

torques, were obtained. The potential advantage of this movement-based estimation procedure for increased accuracy as well as convenience was demonstrated by the less accurately predicted torques based on the CAD-modeled inertial parameters.

The inaccuracy of the CAD-modeled parameters is due to several sources. The links and the motors are complicated, and computing the inertial parameters from the schematic drawing of the manipulator is bound to contain modeling errors. For the DDArm, the masses and moments of inertia are dominated by the large motors at the joints. The modeling of the inertial properties of these motors is difficult since they are made of complicated parts such as the stator windings. Also, the links can be attached to the rotor axes at arbitrary positions by the assembler, introducing uncertainty in the CAD-modeled parameters.

It is possible that the inaccuracy of the CAD-modeled parameters is exaggerated, since the same sensors that were used in the estimation are being used to compare the CAD-modeled parameters to the dynamically estimated parameters. Presumably a systematic error in the sensors, such as a miscalibration of motor torque constants K_T, would be reflected in the dynamically estimated parameters. This would lead to a judgment of better match with these estimated parameters, even though the CAD-modeled parameters could conceivably be more accurate. Ideally an independent measuring procedure, such as weighing and counterbalancing, would be used to resolve this point, but we have not yet done this.

With regard to errors in the motor torque constant, the motors were calibrated with a commercial force/torque sensor, and it is expected that errors in this calibrating device are very small. The potential problems of a dead zone near zero torque and torque ripple (Asada, Youcef-Toumi, and Lim 1984) are not considered to be significant because of the large torques used in this study. Other sources of error are the same as discussed in the previous section and are not repeated here.

Even supposing that there are possible errors in the sensors or kinematic variations due to assembly, the importance of the dynamic estimation of the link inertial parameters is actually emphasized. The controller must deal with the robot kinematics and sensor calibration as they exist, and the estimated model will accommodate kinematic variations and cancel sensor calibration error.

Rigid-body models and the link-inertial parameter estimation method presented in this paper can be applied to a wide range of manipulators, including arms with significant joint and actuator dynamics. Joint dynamics can consist of friction, backlash, and other complex command-to-torque output relations. All that is required to apply this rigid-body parameter estimation method is that the links themselves are rigid and that the torques on these links along the degrees of freedom of the joints be accurately known. If the joint and actuator dynamics are known or are negligible then the link torques can be estimated from the actuator commands. In this paper we estimated the link torques from the motor currents and assumed the joint dynamics were negligible. This assumption was later supported by the success of the estimated model in predicting the joint torques (motor currents) necessary to drive the arm along a particular trajectory. If the joint and actuator dynamics are unknown and substantial, then sensing can be used to measure the torques acting on the links.

4.2.1. Identifiability of Inertial Parameters

There are three groups of inertial parameters: fully identifiable, identifiable in linear combinations, and completely unidentifiable. Membership of a parameter in a group depends on the manipulator's particular geometry. As shown in Table 4 and Appendix I for the DDArm, the 30 inertial parameters are grouped into the following categories:

1. fully identifiable: $m_2c_{x_2}$, I_{xy_2}, I_{xz_2}, $m_3c_{x_3}$, $m_3c_{y_3}$, I_{xy_3}, I_{xz_3}, I_{yz_3}, I_{zz_3},
2. identifiable in linear combinations: I_{zz_1}, $m_2c_{y_2}$, I_{xx_2}, I_{yy_2}, I_{yz_2}, I_{zz_2}, m_3, $m_3c_{z_3}$, I_{xx_3}, I_{yy_3},
3. completely unidentifiable: m_1, $m_1c_{x_1}$, $m_1c_{y_1}$, $m_1c_{z_1}$, I_{xx_1}, I_{xy_1}, I_{xz_1}, I_{yy_1}, I_{yz_1}, m_2, $m_2c_{z_2}$.

Some link inertial parameters are unidentifiable because of restricted motion near the base and the lack of full force-torque sensing at each joint. For the first link, rotation is only possible about its z-axis. Suppose full force-torque sensing is available at joint 1. It can be seen from Eq. (8) that I_{xx_1}, I_{xy_1}, and I_{yy_1} are unidentifiable because they have no effect on joint torque.

Since the gravity vector is parallel to the z-axis, c_{z_1} is also unidentifiable. If it is now supposed that only torque about the z-axis can be sensed, then all inertial parameters for link 1 become unidentifiable except I_{zz_1}.

In a multilink robot a new phenomenon arises. Some parameters can only be identified in linear combinations, because proximal joints must provide the torque sensing to identify fully the parameters of each link. Certain parameters from distal links are carried down to proximal links until a link appears with a rotation axis oriented appropriately for completing the identification. In between, these parameters appear in linear combinations with other parameters. This partial identifiability and the difficulty of analysis become worse as the number of links are increased.

The ridge regression automatically resolves the linear combinations in a least-squares sense, which makes these inertial parameters appear superficially different from those derived by CAD modeling. This is an approximation to computing the pseudoinverse to solve the rank deficient least-squares problem.

Although not as simple as ridge regression, singular value decomposition of $\mathbf{K}$ in Eq. (18) to determine the minimal number of inertial parameters is attractive since it allows reformulating the dynamics with identifiable parameters only. The procedure isolates several sets of parameters whose linear combinations within each set are identifiable. The linear combinations can be reduced by consistently setting certain parameters in these sets to zero, leaving only one nonzero parameter in each set; for example, zeroing m_3, $m_3c_{z_3}$, I_{xx_3}, and I_{xx_2} leaves I_{yz_2}, I_{yy_3}, I_{zz_2}, I_{zz_1}, I_{yy_2}, and $m_2c_{y_2}$ as identifiable parameters. The unidentifiable parameters can also be set to zero. Finally, what remains is a reduced full-rank $\mathbf{K}^T\mathbf{K}$ matrix whose dimension is 15×15.

4.2.2. Model Uncertainty and Control

The degree of uncertainty in inertial parameters is an important factor in judging the robustness of model-based control strategies. Computed torque methods, which involve full dynamics computation (e.g., Luh, Walker, and Paul 1980*a* and 1980*b*), are often criticized for their sensitivity to modeling errors. A variety of alternative robust controllers have been suggested to compensate for presumed modeling errors (Samson 1983; Gilbert and Ha 1984; Spong, Thorp, and Kleinwaks 1984; Slotine 1985). Typically these robust controllers express modeling errors as differential inertia matrix and Coriolis and gravity vectors, but in so doing, no rational basis is provided for the source of errors or the bounds on errors. The error matrices and vectors combine kinematic and dynamic parameter errors, but kinematic calibration is sufficiently developed so that very little error can be expected in the kinematic parameters (Whitney, Lozinski, and Rourke 1984).

One aim of this work was to place similar bounds on inertial parameter errors by explicitly identifying the inertial parameters of each link that go into making the inertia matrix and Coriolis and gravity vectors. Our results in load identification suggest, for example, that mass can be accurately identified to within 1 percent. Therefore, an assumption of 50 percent error in link mass in verifying a robust control formulation (Spong, Thorp, and Kleinwaks 1984) is an unreasonable basis for argument. Slotine (1985) suggests that errors of only a few percent in inertial parameters make his simplified robust controller superior to the computed torque method, but it may well be that these parameters can be identified more accurately than his assumptions.

We are currently studying the effectiveness of different control algorithms and their robustness to modelling errors, given the estimated dynamic model. The customized dynamic equations with reduced inertial parameters will be used to increase the computational efficiency by taking further advantage of particularized kinematic and dynamic features, in this case the zeroed inertial parameters (Hollerbach and Sahar 1983). Finally, this analysis is being extended to include flexibility in joint transmission elements and in link structures.

Acknowledgments

We would like to thank Steve Jacobsen for advice on ridge regression, and V. T. Rajan for evaluating the integral approach to load estimation.

Appendix I

The customized closed-form equations of the dynamics of the MIT Serial Link Direct Drive Arm are presented here. To simplify the equations, the following notation is used: $s_2 = \sin\theta_2$, $s_3 = \sin\theta_3$, $c_2 = \cos\theta_2$, $c_3 = \cos\theta_3$. Also, $g = 9.80665\ \text{m/s}^2$. The closed-form equations are:

$$
\begin{aligned}
n_1 = {} & \mathrm{SP}_4(\ddot{\theta}_1) + \mathrm{SP}_5(2\dot{\theta}_1\dot{\theta}_2 s_2 c_2 - \ddot{\theta}_1 c_2^2) \\
& + I_{xy_2}(2\ddot{\theta}_1 s_2 c_2 - 2\dot{\theta}_1\dot{\theta}_2 + 4\dot{\theta}_1\dot{\theta}_2 c_2^2) \\
& + I_{xz_2}(\ddot{\theta}_2 s_2 + v_2^2 c_2) + \mathrm{SP}_1(\ddot{\theta}_2 c_2 - v_2^2 s_2) \\
& + m_3 c_{x_3}(l_2)(2\ddot{\theta}_1 s_3 + 2\dot{\theta}_2\dot{\theta}_3 s_2 s_3 - \ddot{\theta}_3 s_3 c_2 \\
& + 2\dot{\theta}_1\dot{\theta}_3 c_3 - \ddot{\theta}_2 s_2 c_3 - v_2^2 c_2 c_3 - v_3^2 c_2 c_3) \\
& + m_3 c_{y_3}(l_2)(\ddot{\theta}_2 s_2 s_3 - 2\dot{\theta}_1\dot{\theta}_3 s_3 + v_2^2 s_3 c_2 \\
& + v_3^2 s_3 c_2 + 2\ddot{\theta}_1 c_3 + 2\dot{\theta}_2\dot{\theta}_3 s_2 c_3 - \ddot{\theta}_3 c_2 c_3) \\
& + \mathrm{SP}_2(\ddot{\theta}_1 c_2^2 - \ddot{\theta}_1 - \dot{\theta}_2\dot{\theta}_3 s_2 - 2\dot{\theta}_1\dot{\theta}_2 s_2 c_2 \\
& - 2\dot{\theta}_1\dot{\theta}_3 s_3 c_3 + \ddot{\theta}_2 s_2 s_3 c_3 \\
& + v_2^2 s_3 c_2 c_3 + 2\dot{\theta}_1\dot{\theta}_3 s_3 c_2^2 c_3 + \ddot{\theta}_1 c_3^2 \\
& + 2\dot{\theta}_2\dot{\theta}_3 s_2 c_3^2 + 2\dot{\theta}_1\dot{\theta}_2 s_2 c_2 c_3 c_3 - \ddot{\theta}_1 c_2^2 c_3 c_3) \\
& + I_{xy_3}(2\dot{\theta}_1\dot{\theta}_3 - \ddot{\theta}_2 s_2 - v_2^2 c_2 - 2\dot{\theta}_1\dot{\theta}_3 c_2^2 \\
& - 2\ddot{\theta}_1 s_3 c_3 - 4\dot{\theta}_2\dot{\theta}_3 s_2 s_3 c_3 \\
& - 4\dot{\theta}_1\dot{\theta}_2 s_2 s_3 c_2 c_3 + 2\ddot{\theta}_1 s_3 c_2^2 c_3 - 4\dot{\theta}_1\dot{\theta}_3 c_3^2 \\
& + 2\ddot{\theta}_2 s_2 c_3^2 + 2\dot{\theta}_2\dot{\theta}_2 c_2 c_3^2 + 4\dot{\theta}_1\dot{\theta}_3 c_2 c_2 c_3^2) \\
& + I_{xz_3}(\ddot{\theta}_2\dot{\theta}_2 s_2 s_3 - v_3^2 s_2 s_3 - \ddot{\theta}_2 s_3 c_2 + 2\dot{\theta}_1\dot{\theta}_3 s_2 s_3 c_2 \\
& + 2\dot{\theta}_1\dot{\theta}_2 c_3 + \ddot{\theta}_3 s_2 c_3 - 2\ddot{\theta}_1 s_2 c_2 c_3 - 4\dot{\theta}_1\dot{\theta}_2 c_2^2 c_3) \\
& + I_{yz_3}(2\ddot{\theta}_1 s_2 s_3 c_2 - 2\dot{\theta}_1\dot{\theta}_2 s_3 - \ddot{\theta}_3 s_2 s_3 + 4\dot{\theta}_1\dot{\theta}_2 s_3 c_2^2 \\
& + v_2^2 s_2 c_3 - v_3^2 s_2 c_3 - \ddot{\theta}_2 c_2 c_3 + 2\dot{\theta}_1\dot{\theta}_3 s_2 c_2 c_3) \\
& + I_{zz_3}(\dot{\theta}_2\dot{\theta}_3 s_2 - \ddot{\theta}_3 c_2 - 2\dot{\theta}_1\dot{\theta}_2 s_2 c_2 + \ddot{\theta}_1 c_2^2).
\end{aligned}
$$

$$
\begin{aligned}
n_2 = {} & m_2 c_{x_2}(g c_2) + \mathrm{SP}_6(g s_2) - \mathrm{SP}_5(v_1^2 s_1 c_2) \\
& + I_{xy_2}(v_1^2 - 2v_1^2 c_2^2) + I_{xz_2}(\ddot{\theta}_1 s_2) \\
& + \mathrm{SP}_1(\ddot{\theta}_1 c_2) + \mathrm{SP}_3(\ddot{\theta}_2) + m_3 c_{x_3}(g c_2 c_3 - l_2\ddot{\theta}_1 s_2 c_3) \\
& + m_3 c_{y_3}(l_2\ddot{\theta}_1 s_2 s_3 - g s_3 c_2) \\
& + \mathrm{SP}_2(\dot{\theta}_1\dot{\theta}_1 s_2 c_2 - \dot{\theta}_1\dot{\theta}_3 s_2 + 2\dot{\theta}_2\dot{\theta}_3 s_3 c_3 + \ddot{\theta}_1 s_2 s_3 c_3 \\
& - \ddot{\theta}_2 c_3^2 + 2\dot{\theta}_1\dot{\theta}_3 s_2 c_3^2 - \dot{\theta}_1\dot{\theta}_1 s_2 c_2 c_3^2) \\
& + I_{xy_3}(2\ddot{\theta}_2 s_3 c_3 - 2\dot{\theta}_2\dot{\theta}_3 - \ddot{\theta}_1 s_2 - 4\dot{\theta}_1\dot{\theta}_3 s_2 s_3 c_3 \\
& + 2v_1^2 s_2 s_3 c_2 c_3 + 4\dot{\theta}_2\dot{\theta}_3 c_3^2 + 2\ddot{\theta}_1 s_2 c_3^2) \\
& + I_{xz_3}(\ddot{\theta}_3 s_3 - \ddot{\theta}_1 s_3 c_2 - v_1^2 c_3 + v_3^2 c_3 \\
& - 2\dot{\theta}_1\dot{\theta}_3 c_2 c_3 + 2v_1^2 c_2^2 c_3) \\
& + I_{yz_3}(v_1^2 s_3 - v_3^2 s_3 + 2\dot{\theta}_1\dot{\theta}_3 s_3 c_2 - 2v_1^2 s_3 c_2^2 \\
& + \ddot{\theta}_3 c_3 - \ddot{\theta}_1 c_2 c_3) \\
& + I_{zz_3}(v_1^2 s_2 c_2 - \ddot{\theta}_1\dot{\theta}_3 s_2).
\end{aligned}
$$

$$
\begin{aligned}
n_3 = {} & m_3 c_{x_3}(-g s_2 s_3 - l_2\ddot{\theta}_1 s_3 c_2 - l_2 v_1^2 c_3) \\
& + m_3 c_{y_3}(l_2 v_1^2 s_3 - l_2\ddot{\theta}_1 c_2 c_3 - g s_2 c_3) \\
& + \mathrm{SP}_2(\ddot{\theta}_1\dot{\theta}_2 s_2 + v_1^2 s_3 c_3 - v_2^2 s_3 c_3 - v_1^2 s_3 c_3 c_2^2 \\
& - 2\dot{\theta}_1\dot{\theta}_2 s_2 c_3^2) \\
& + I_{xy_3}(v_2^2 - v_1^2 + v_1^2 c_2^2 + 4\dot{\theta}_1\dot{\theta}_2 s_2 s_3 c_3 \\
& + 2v_1^2 c_3^2 - 2v_2^2 c_3^2 - 2v_1^2 c_2^2 c_3^2) \\
& + I_{xz_3}(\ddot{\theta}_2 s_3 - v_1^2 s_2 s_3 c_2 + \ddot{\theta}_1 s_2 c_3 + 2\dot{\theta}_1\dot{\theta}_2 c_2 c_3) \\
& + I_{yz_3}(\ddot{\theta}_2 c_3 - \ddot{\theta}_1 s_2 s_3 - 2\dot{\theta}_1\dot{\theta}_2 s_3 c_2 - v_1^2 s_2 c_2 c_3) \\
& + I_{zz_3}(\ddot{\theta}_3 + \dot{\theta}_1\dot{\theta}_2 s_2 - \ddot{\theta}_1 c_2).
\end{aligned}
$$

In these equations, there are 15 reduced inertial parameters: $m_2 c_{x_2}$, I_{xy_2}, I_{xz_2}, $m_3 c_{x_3}$, $m_3 c_{y_3}$, I_{xy_3}, I_{xz_3}, I_{yz_3}, I_{zz_3}, SP_1, SP_2, SP_3, SP_4, SP_5, SP_6. The SP_i variables are abbreviations for the following linear combinations:

$$
\begin{aligned}
\mathrm{SP}_1 &= m_3 c_{z_3} l_2 + I_{yz_2}, \\
\mathrm{SP}_2 &= I_{xx_3} - I_{yy_3}, \\
\mathrm{SP}_3 &= I_{zz_2} + I_{xx_3}, \\
\mathrm{SP}_4 &= I_{zz_1} + I_{xx_2} + I_{xx_3} + m_3 l_2^2, \\
\mathrm{SP}_5 &= I_{xx_2} + I_{xx_3} - I_{yy_2}, \\
\mathrm{SP}_6 &= m_3 c_{z_3} - m_2 c_{y_2}.
\end{aligned}
$$

Eleven inertial parameters do not appear in these equations at all and are completely unidentifiable: m_1, $m_1 c_{x_1}$, $m_1 c_{y_1}$, $m_1 c_{z_1}$, I_{xx_1}, I_{xy_1}, I_{xz_1}, I_{yy_1}, I_{yz_1}, m_2, $m_2 c_{z_2}$.

Appendix II

In this appendix the integral form of the equations for load estimation are derived from Eqs. (4) and (7). First, $\ddot{\mathbf{p}}$ may be written as (Symon 1971):

$$
\mathbf{R}\frac{d}{dt}({}^o\dot{\mathbf{p}}) = \frac{d}{dt}(\mathbf{R}\cdot{}^o\dot{\mathbf{p}}) + \mathbf{R}({}^o\boldsymbol{\omega}\times{}^o\dot{\mathbf{p}}), \qquad \text{(A1)}
$$

where ${}^o\mathbf{p}$ is expressed in the inertial coordinate system and ${}^p\mathbf{p}$ in the force-sensor coordinate system. $\mathbf{R}$ is the rotation matrix from the inertial coordinate system to the force-sensing coordinate system. Integration yields:

$$
\begin{aligned}
\int_t^{t+T} \mathbf{R}\cdot{}^o\ddot{\mathbf{p}}\,d\tau &= (\mathbf{R}\cdot{}^o\dot{\mathbf{p}})\Big|_t^{t+T} \\
&\quad + \int_t^{t+T} \mathbf{R}({}^o\boldsymbol{\omega}\times{}^o\dot{\mathbf{p}})d\tau
\end{aligned} \qquad \text{(A2)}
$$

and after performing the indicated rotations,

$$\int_t^{t+T} {}^p\dot{\mathbf{p}}\, d\tau = {}^p\dot{\mathbf{p}}\Big|_t^{t+T} + \int_t^{t+T} {}^p\boldsymbol{\omega} \times {}^p\dot{\mathbf{p}}\, d\tau. \quad \text{(A3)}$$

Similarly

$$\begin{aligned}\int_t^{t+T} {}^p\dot{\boldsymbol{\omega}}\, d\tau &= {}^p\boldsymbol{\omega}\Big|_t^{t+T} + \int_t^{t+T} {}^p\boldsymbol{\omega} \times {}^p\boldsymbol{\omega}\, d\tau \\ &= {}^p\boldsymbol{\omega}\Big|_t^{t+T}\end{aligned} \quad \text{(A4)}$$

since $\boldsymbol{\omega} \times \boldsymbol{\omega} = 0$, and

$$\int_t^{t+T} {}^p\mathbf{g}\, d\tau = \left(\int_t^{t+T} \mathbf{R}\, d\tau\right) {}^o\mathbf{g}. \quad \text{(A5)}$$

Each of the matrices $[{}^p\dot{\boldsymbol{\omega}}\times]$ and $[\,\cdot\,\dot{\boldsymbol{\omega}}]$ can be integrated element by element to show that

$$\begin{aligned}\int_t^{t+T} [{}^p\dot{\boldsymbol{\omega}}\times] d\tau &= \left[\left(\int_t^{t+T} {}^p\dot{\boldsymbol{\omega}}\, d\tau\right)\times\right] \\ &= \left[\left({}^p\boldsymbol{\omega}\Big|_t^{t+T}\right)\times\right],\end{aligned} \quad \text{(A6)}$$

$$\begin{aligned}\int_t^{t+T} [\,\cdot\,{}^p\dot{\boldsymbol{\omega}}] d\tau &= \left[\,\cdot\,\left(\int_t^{t+T} {}^p\dot{\boldsymbol{\omega}}\, d\tau\right)\right] \\ &= \left[\,\cdot\,\left({}^p\boldsymbol{\omega}\Big|_t^{t+T}\right)\right].\end{aligned} \quad \text{(A7)}$$

The matrix $[(\mathbf{g} - \ddot{\mathbf{p}})\times]$ is integrated similarly, while $[{}^p\boldsymbol{\omega}\times][{}^p\boldsymbol{\omega}\times]$ and $[{}^p\boldsymbol{\omega}\times][\,\cdot\,{}^p\boldsymbol{\omega}]$ are numerically integrated by adding values at each time step. The results are given in Eq. (25).

References

An, C. H., Atkeson, C. G., and Hollerbach, J. M. 1985 (Dec. 11–13, Fort Lauderdale). Estimation of inertial parameters of rigid-body links of manipulators. *Proc. 24th IEEE Conf. Decision and Contr.*, pp. 990–995.

Asada, H., and Youcef-Toumi, K. 1984. Analysis and design of a direct-drive arm with a five-bar-link parallel drive mechanism. *ASME J. Dyn. Sys., Meas., Contr.* 106:225–230.

Asada, H., Youcef-Toumi, K., and Lim, S. K. 1984 (Dec. 12–14, Las Vegas). Joint torque measurement of a direct-drive arm. *Proc. 23rd IEEE Conf. Decision and Contr.*, pp. 1332–1337.

Atkeson, C. G., An, C. H., and Hollerbach, J. M. 1985*a* (October 7–11, Gouvieux [Chantilly], France). Estimation of inertial parameters of manipulator loads and links. *Preprints of 3rd Int. Symp. Robotics Res.*, pp. 32–39.

Atkeson, C. G., An, C. H., and Hollerbach, J. M. 1985*b* (Dec. 11–13, Fort Lauderdale). Rigid-body load identification for manipulators. *Proc. 24th Conf. Decision and Contr.*, pp. 996–1002.

Coiffet, P. 1983. *Robot technology: interaction with the environment, vol. 2.* Englewood Cliffs, N.J.: Prentice-Hall.

Gelb, A., ed. 1974. *Applied optimal estimation.* Cambridge: MIT Press.

Gilbert, E. G., and Ha, I. J. 1984. An approach to nonlinear feedback control with applications to robotics. *IEEE Trans. Sys., Man, Cyber.* SMC-14:879–884.

Golub, G. H., and Van Loan, C. F. 1983. *Matrix computations.* Baltimore: Johns Hopkins University Press.

Hollerbach, J. M., and Sahar, G. 1983. Wrist-partitioned inverse kinematic accelerations and manipulator dynamics. *Int. J. Robotics Res.* 2(4):61–76.

Lawson, C. L., and Hanson, R. J. 1974. *Solving least-squares problems.* Englewood Cliffs, N.J.: Prentice-Hall.

Lee, K. 1983 (Dec.). Shape optimization of assemblies using geometric properties. Ph.D. thesis, Massachusetts Institute of Technology, Mechanical Engineering Department.

Ljung, L., and Soderstrom, T. 1983. *Theory and practice of recursive identification.* Cambridge: MIT Press.

Luh, J. Y. S., Walker, M. W., and Paul, R. P. 1980*a*. On-line computational scheme for mechanical manipulators. *J. Dyn. Sys., Meas., Contr.* 102:69–76.

Luh, J. Y. S., Walker, M. W., and Paul, R. P. 1980*b*. Resolved-acceleration control of mechanical manipulators. *IEEE Trans. Auto. Contr.* AC-25:468–474.

Marquardt, D. W., and Snee, R. D. 1975. Ridge regression in practice. *Amer. Statistician* 29:3–20.

Mathlab Group. 1983. MACSYMA Reference Manual. Version 10. Cambridge, Mass.: Massachusetts Institute of Technology, Laboratory for Computer Science.

Mayeda, H., Osuka, K., and Kangawa, A. 1984 (July 2–6, Budapest). A new identification method for serial manipulator arms. *Preprints IFAC 9th World Congress, Vol. VI*, pp. 74–79.

Mukerjee, A. 1984 (Nov., Cambridge, Mass.). Adaptation in biological sensory-motor systems: a model for robotic control. *Proc. SPIE Conf. on Intelligent Robots and Computer Vision, Vol. 521.* Cambridge, Mass.

Mukerjee, A., and Ballard, D. H. 1985 (Mar. 25–28, St.

Louis). Self-calibration in robot manipulators. *Proc. IEEE Conf. Robotics and Automation* pp. 1050–1057.

Neuman, C. P., and Khosia, P. K. 1985 (May 29–31, New Haven). Identification of robot dynamics: an application of recursive estimation. *Proc. 4th Yale Workshop on Applications of Adaptive Sys. Theory,* pp. 42–49.

Olsen, H. B., and Bekey, G. A. 1985 (Mar. 25–28, St. Louis). Identification of parameters in models of robots with rotary joints. *Proc. IEEE Conf. Robotics and Automation,* pp. 1045–1050.

Paul, R. P. 1981. *Robot manipulators: mathematics, programming, and control.* Cambridge: MIT Press.

Samson, C. 1983 (Dec. 14–16, San Antonio). Robust nonlinear control of robotic manipulators. *Proc. 22nd IEEE Conf. Decision and Contr.*

Slotine, J.-J. E. 1985. The robust control of robot manipulators. *Int. J. Robotics Res.* 4(2):49–64.

Spong, M. W., Thorp, J. S., and Kleinwaks, J. M. 1984 (Dec. 12–14, Las Vegas). The control of robot manipulators with bounded input. Part II: robustness and disturbance rejection. *Proc. 23rd IEEE Conf. Decision and Contr.,* pp. 1047–1052.

Symon, K. R. 1971. *Mechanics.* Reading, Mass.: Addison-Wesley.

Whitney, D. E., Lozinski, C. A., and Rourke, J. M. 1984. Industrial robot calibration method and results. CSDL-P-1879. Cambridge, Mass.: Charles Stark Draper Laboratory.